arXiv:1405.2152v1 [cond-mat.mtrl-sci] 9 May 2014

Spin Spirals in Surface Alloys on Ru(0001): A First-principles Study

Sananda Biswas,[1] Gustav Bihlmayer,[2] Shobhana Narasimhan,[1,3] and Stefan Blügel[2]

[1]*Theoretical Sciences Unit, Jawaharlal Nehru Centre for Advanced Scientific Research, Jakkur, Bangalore, India*
[2]*Peter Grünberg Institut and Institute for Advanced Simulation, Forschungszentrum Jülich and JARA, 52425 Jülich, Germany*
[3]*Sheikh Saqr Laboratory, ICMS, Jawaharlal Nehru Centre for Advanced Scientific Research, Jakkur, Bangalore, India*

(Dated: May 12, 2014)

We have used *ab initio* density functional theory to compute the magnetic ground states of the surface alloy systems $FeAu_2$/Ru(0001) and $MnAu_2$/Ru(0001). For both systems, we find that the lowest energy magnetic configuration corresponds to a left-rotating spin spiral, in which the sense of rotation is determined by the Dzyaloshinskii-Moriya interaction. These spirals are lower in energy than the ferromagnetic configuration by 3–4 meV per nm^2. We also find that $FeAu_2$/Ru(0001) has a significantly high magnetic anisotropy energy, of the order 1 meV per Fe atom. By comparing with the corresponding freestanding alloy monolayers, we find that the presence of the Ru substrate plays a significant role in determining the magnetic properties of the surface alloy systems.

PACS numbers: 75.70.-i, 75.70.Ak, 75.25.-j

I. INTRODUCTION

The spin-orbit interaction in magnetic systems leads to the possibility of stabilizing exotic non-collinear magnetic structures, such as spin spirals induced by the Dzyaloshinskii-Moriya (DM) interaction.[1,2] The recent emergence of the field of spintronics has led to additional interest in such systems. As an example, it has been suggested that the spin torque arising from the flow of a spin-polarized current through a system where the spins are arranged in a chiral fashion can lead to various phenomena such as the switching of magnetization, and microwave emission.[3,4] The Spin-orbit interaction can also lead to obtaining magnetic structures with significantly enhanced magnetic anisotropy energy (MAE).[5] The MAE is defined as the energy barrier that has to be overcome to orient the magnetization oppositely, along the easy axis, by rotating it through a hard axis; for information storage applications, it is crucial that it should have a high value, so that stored data is not lost through thermal fluctuations. In this work, we use *ab initio* density functional theory to explore such issues for ultrathin surface alloys, created by the co-deposition of two bulk-immiscible elements on a substrate.

In a spin spiral, the moments on all magnetic atoms have approximately the same magnitude, but their direction rotates by a phase factor as one proceeds from one atom to the next, along the direction of propagation. Only a few thin-film systems have been shown to display a spin spiral ground state: single and double layers of Mn on W(110),[6,7] a single monolayer of Mn on W(001),[8] a double monolayer of Fe on W(110),[9] and a PdFe bilayer on Ir(111).[10] It is therefore appealing to see whether alloying can lead to more systems of this kind.

Surface alloys are systems where two or more elements form an alloy restricted to the surface layer alone. Recent interest in such systems has been particularly boosted by the finding that it is possible to form surface alloys out of elements that are immiscible in the bulk.[11,12] In early work, it was believed that the driving force for alloy formation in such systems was primarily the relief of surface stress.[13] However, more recently it has been shown that when one of the constituents is a magnetic element, the dominant effect in driving mixing can, in some cases, be magnetism.[14,15]

In this study, we focus on two supported systems, $FeAu_2$/Ru(0001) and $MnAu_2$/Ru(0001). In order to better distinguish those effects that arise from the presence of the Ru substrate, we also consider two hypothetical systems, viz., a freestanding $FeAu_2$ monolayer, and a freestanding $MnAu_2$ monolayer, both maintained at a nearest-neighbor spacing equal to that in bulk Ru. Ru crystallizes in the hexagonal close packed (hcp) structure, and thus the Ru(0001) surface has a triangular lattice, which offers an ideal substrate to study magnetic frustration, which can lead to a variety of interesting magnetic structures. Fe and Mn are both magnetic elements, but while bulk Fe is ferromagnetic, bulk α-Mn is non-collinear antiferromagnetic at room temperature.[16] Moreover, while Fe and Au are bulk-immiscible, Mn and Au form bulk alloys, such as $MnAu_2$, which displays a helical arrangement of the spins on Mn atoms.[17,18] When a monolayer of Fe is deposited on Ru(0001), the resulting Fe/Ru(0001) system has a 120° Néel state.[19] In contrast, Mn/Ru(0001) displays a row-wise antiferromagnetic structure.[20] $FeAu_2$/Ru(0001) has been shown, both experimentally and theoretically,[15] to have a pseudomorphic $(\sqrt{3} \times \sqrt{3})$ structure, with long-range-order. In this structure, the Fe atoms in the overlayer constitute a triangular superlattice, and every Fe atom is surrounded by six Au atoms [see Fig. 1(a)]. It has been shown, by density functional theory calculations, that this structure is stabilized primarily by magnetism

rather than stress relief.[15] $MnAu_2$/Ru(0001) has a similar structure, with the Fe atoms replaced by Mn atoms. We have found that this structure is also stable against phase-segregation.[21] The presence of Au and Ru atoms is interesting for our purpose, since they are expected to enhance spin-orbit coupling, and thus increase both the DM interaction and the MAE.

The outline of this paper is as follows. In Section II, we describe the four systems on which we have carried out our calculations. Next, in Section IIIA, we lay out the relevant formalism, describing separately each of the three main contributions to the total energy, viz., the symmetric Heisenberg exchange energy, the Dzyaloshinskii-Moriya energy, and the magnetic anisotropy energy. Next, in Section IIIB, we give the technical details of our calculations. Our results are presented in Section IV. Section V contains a discussion of our results. We present a summary in Section VI. In an appendix, we discuss issues related to the applicability of the force theorem.

II. SYSTEMS

As mentioned above, in order to clearly separate out the effects of the substrate, we perform calculations on $X\mathrm{Au}_2$ layers (X = Fe or Mn), both with and without the Ru(0001) substrate. Thus, we have studied four systems: (A) freestanding $FeAu_2$ monolayer, (B) freestanding $MnAu_2$ monolayer, (C) $FeAu_2$/Ru(0001), and (D) $MnAu_2$/Ru(0001). Note that in all four cases, the in-plane nearest-neighbor spacing is fixed as equal to the experimental value for Ru(0001) = 2.70 Å.

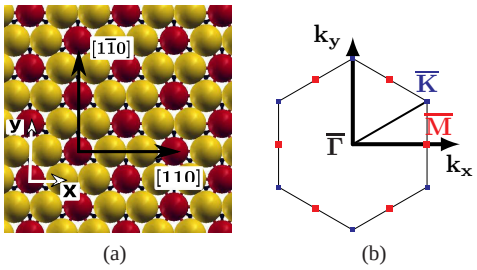

(a) (b)

FIG. 1. (Color online) System geometry in real and reciprocal space: (a) shows the top view of the alloy monolayer, $X\mathrm{Au}_2$, (X = Fe or Mn) on Ru(0001). The dark (red) and light (yellow) spheres represent X and Au atoms, respectively. The black dots indicate the topmost layer of the Ru atoms, for those systems in which the Ru substrate is present. (b) shows the corresponding hexagonal surface Brillouin zone and the high symmetry points $\overline{\Gamma}$, $\overline{\mathrm{M}}$, and $\overline{\mathrm{K}}$.

Fig. 1(a) shows the top view of all four systems. The corresponding surface Brillouin zone, along with high symmetry points, is shown in Fig. 1(b). When computing spin spirals with wavevector $\mathbf{q}$, the $\overline{\Gamma}$ point (zone center) corresponds to the ferromagnetic state, $\overline{\mathrm{K}}$ corresponds to a row-wise antiferromagnetic state, and $\overline{\mathrm{M}}$ corresponds to a 120° Néel state. Points in the interior of the Brillouin zone correspond to general spin spirals.

III. METHOD

A. Formalism

For a spin spiral with wavevector $\mathbf{q}$, the magnetic moment of a magnetic atom at position $\mathbf{R}$ is given by:

$$\mathbf{m}(\mathbf{R}) = m \begin{pmatrix} \sin\alpha\, \cos(\mathbf{q}\cdot\mathbf{R}) \\ \sin\alpha\, \sin(\mathbf{q}\cdot\mathbf{R}) \\ \cos\alpha \end{pmatrix}, \tag{1}$$

where m is the magnitude of the magnetic moment, and α is the cone angle of the spin spiral. The total energy of such a spin spiral is given by the sum of three terms:

$$E_{\mathrm{total}}(\mathbf{q}) = E_{\mathrm{HE}}(\mathbf{q}) + E_{\mathrm{DM}}(\mathbf{q}) + K_{\mathrm{avg}}. \tag{2}$$

In Eq. (2), the first term on the right-hand-side, E_{HE}, is the energy due to symmetric Heisenberg exchange. The second term, E_{DM}, arises from the Dzyaloshinskii-Moriya interaction. The third term, K_{avg}, denotes the average value of the MAE over one wavelength λ of the spin spiral. Note that in the absence of spin-orbit coupling, only the first of these three terms would be present (magnetic dipole-dipole interactions in low-dimensional systems generally being very weak). Throughout this paper, the zero of energy is defined such that $E_{\mathrm{HE}}(\mathbf{q}=0) = 0$. As $|\mathbf{q}| = 2\pi/\lambda$, we can also write Eq. (2) as a function of λ^{-1}.

In this paper, we restrict ourselves to considering only homogeneous, cycloidal, planar spin spirals. In homogeneous spin spirals the relative angle between neighboring spins is always a constant. In order to describe a spin spiral, in addition to a wavevector $\mathbf{q}$, one must specify an axis about which the spins rotate. In helical spin spirals, this axis of rotation is parallel to $\mathbf{q}$, whereas in cycloidal spin spirals, it is perpendicular to $\mathbf{q}$. Symmetry arguments predict that, on an isotropic surface, cycloidal spin spirals will always be lower in energy than helical spin spirals.[8,22] In planar spin spirals, the spins are confined to a plane normal to the rotation-axis; the Dzyaloshinskii-Moriya interaction is expected to be largest in such a situation.[1,23]

Below, we describe each of the terms contributing to the total energy in Eq. (2).

1. *Heisenberg Exchange Energy E_{HE}*

If we consider a system consisting of spins $\{\mathbf{S}_i\}$, on lattice sites i, then one can write the contribution to the total energy from the Heisenberg exchange interaction as:

$$E_{\mathrm{HE}} = -\sum_{i<j} J_{ij}(\mathbf{S}_i \cdot \mathbf{S}_j), \tag{3}$$

where J_{ij} is the exchange integral and the sum runs over all pairs of distinct lattice sites i and j. Note that this interaction is symmetric with respect to exchange of spins between sites.

To calculate $E_{\rm HE}$ for a spin spiral with wavevector $\mathbf{q} \neq 0$ requires, in principle, the use of a supercell. This would hugely increase the computational time, especially for spin spirals of long wavelength. However, the use of supercells can be avoided by making use of the generalized Bloch theorem;[24] this permits one to carry out all calculations making use of the chemical unit cell.

There are two possible approaches for calculating $E_{\rm HE}$. The quicker, but less accurate way, is to make use of Andersen's force theorem, also referred to as the magnetic force theorem or frozen force theorem.[25] This states that the change in energy due to the presence of a small perturbation can be calculated non-self-consistently from the eigenvalue sum, if the self-consistent solution of the unperturbed Hamiltonian is known. It is generally assumed that the force theorem can be applied for most small perturbations, and can be used, e.g., to calculate the energy difference $\delta E_{\rm HE}$ between two spin spirals of slightly different wavelengths, or the MAE.

The more time-consuming, but also more accurate, approach for calculating $E_{\rm HE}$ is to perform fully self-consistent calculations. In this approach, the ground state electronic and magnetic densities (n_0, $\mathbf{m}_0$) are calculated self-consistently for each spin spiral, so as to yield a precise value for the energy difference $\delta E_{\rm HE}$ between two spin spirals of different wavelengths.

Given the wide use of the force theorem in calculations of magnetic structure, it would be of interest to obtain some insight into its domain of applicability, and to examine how accurate results obtained using it, are. For this reason, we have used both the force theorem and self-consistent approaches in this paper, and present a comparison of results obtained using the two techniques.

2. *Dzyaloshinskii-Moriya Energy $E_{\rm DM}$*

In an inversion-asymmetric system, such as a surface, not only the symmetric Heisenberg exchange interaction, but also the antisymmetric exchange (DM) interaction becomes important, and can play a crucial role in determining the magnetic ground state of the system.[1,2] The energy due to the DM interaction can be written as:

$$E_{\rm DM} = \sum_{i<j} \mathbf{D}_{ij} \cdot (\mathbf{S}_i \times \mathbf{S}_j), \tag{4}$$

where $\mathbf{D}_{ij}$ is the DM vector, and the sum again runs over distinct lattice sites. It has been shown that depending on the symmetry of a system, some or all components of $\mathbf{D}$ may vanish.[22] The non-zero components of $\mathbf{D}$ can be obtained by spin spiral calculations varying $\mathbf{q}$ along different crystallographic directions. For planar cycloidal spin spirals on a surface, such as those considered in this study, the component of $\mathbf{D}$ along $\mathbf{q}$ vanishes by symmetry. However, non-zero components of $\mathbf{D}$, which are orthogonal to $\mathbf{q}$, may exist. For example, if $\mathbf{q}$ lies along the x-axis ([110] direction), the non-zero components of $\mathbf{D}$ can be D_y and D_z, whereas, if $\mathbf{q}$ lies along the y-axis ([1$\bar{1}$0] direction), then the non-zero components can be D_x and D_z [see Fig. 1(a)]. Note that we find that the freestanding $FeAu_2$ and $MnAu_2$ monolayers remain completely flat, i.e., display no buckling, and thus, by symmetry, the DM interaction is absent for these systems.

To obtain $E_{\rm DM}$, one can solve the Dirac equation self-consistently. To do this one would, in principle, need to use large supercells, as the generalized Bloch theorem breaks down in the presence of spin-orbit coupling. However, to deal with this problem, a technique has been developed[26] to obtain $E_{\rm DM}$ within the chemical unit cell, treating the spin-orbit coupling as a small perturbation to first order. We have employed this method for calculating $E_{\rm DM}$.

3. *Magnetic Anisotropy Energy K*

The magnetic anisotropy energy (MAE) is the height of the energy barrier that has to be overcome to reverse the direction of the spin along the easy axis, and is given by:

$$K = E^{\text{hard-axis}} - E^{\text{easy-axis}}, \tag{5}$$

where $E^{\text{hard-axis}}$ and $E^{\text{easy-axis}}$ are the total energies of the system with magnetization along the hard-axis and the easy-axis, respectively, in the plane of rotation of the spins. The MAE (K) has two contributions, $K_{\rm SO}$ and $K_{\rm dip}$, arising from the spin-orbit (SO) coupling and the magnetic dipole-dipole interaction, respectively.

One can perform either self-consistent calculations or use the force theorem to obtain the value of K. We have used both methods and compared the results.

B. Calculation Details

We have used density functional theory (DFT) as implemented in the FLEUR code,[27] which is based on the Full-potential Linearized Augmented Plane-wave (FLAPW) method. Exchange-correlation interactions were treated using a generalized gradient approximation of the Perdew-Burke-Ernzerhof form.[28] The muffin-tin radii of Mn, Fe, Au and Ru were set equal to 2.56, 2.32, 2.42, and 2.32 a.u., respectively. The cutoff for the ℓ-value of the basis set consisting of spherical harmonics was fixed at 12, in order to expand the wavefunction inside the muffin-tins, while the ℓ-cutoff for the non-spherical part of the Hamiltonian was chosen to be 8. The plane-wave cutoff for the basis set used to expand the electronic wavefunction in the interstitial region was 3.6 a.u.$^{-1}$; this was increased to 4 a.u.$^{-1}$ when calculating the MAE, in order to achieve the

increased accuracy necessary here. For the charge density and the exchange-correlation part of the potential, the plane-wave cutoffs were 12.3 a.u.$^{-1}$ and 10.3 a.u.$^{-1}$, respectively.

We have considered two collinear magnetic configurations: ferromagnetic (FM) and row-wise AFM. For the freestanding XAu$_2$ monolayer systems, the chemical (primitive) unit cell contains three atoms: one X atom and two Au atoms. All the calculations for the XAu$_2$ alloy monolayers were carried out within this unit cell, except while performing collinear magnetic calculations for the antiferromagnetic (AFM) state. For these calculations a rectangular supercell, containing two X atoms and four Au atoms, was used. All the atoms were relaxed until the forces on each atom were less than 1 mHa/a.u. In both the FM and row-wise AFM configurations, we found that the freestanding FeAu$_2$ and MnAu$_2$ monolayers remained completely flat upon relaxation, i.e., no buckling was observed.

For the XAu$_2$/Ru(0001) systems, the Ru(0001) substrate was modeled by a slab containing six atomic layers of Ru. For geometric optimization and MAE calculations, a symmetric slab was used, in which the alloy monolayer was placed on both sides of the slab. When optimizing geometries, the alloy layers and the first two Ru layers were allowed to relax, with the same force convergence criterion as used for the freestanding monolayers. To calculate $E_{\rm HE}$ and $E_{\rm DM}$ in an inversion-asymmetric environment, an asymmetric slab was used, in which the alloy monolayer was deposited on only the upper surface of the six-layer Ru slab.

We found that for XAu$_2$/Ru(0001), the atoms on the overlayer buckled upon relaxation, in both FM and row-wise AFM configurations. Being larger, the Au atoms relax further away from the substrate, while the smaller X atoms remain closer to the substrate; the degree of buckling is quite significant. In order to quantify the degree of buckling, we computed $d_{\rm b} = d_{\rm Au} - d_X$, where $d_{\rm Au}$ and d_X are the z coordinates of the Au and X atoms, respectively. We found that for FeAu$_2$/Ru(0001), $d_{\rm b} = 0.38$ Å for both FM and AFM configurations, while for MnAu$_2$/Ru(0001), the values of $d_{\rm b}$ were 0.22 Å and 0.27 Å in the FM and row-wise AFM configurations, respectively. This buckling plays an important role in the DM interaction, as we will see further below.

The interlayer distance along the z-direction between the X atom and the first Ru layer is 2.12 Å for FeAu$_2$/Ru(0001) and 2.30 Å for MnAu$_2$/Ru(0001). The larger value in the latter case can be attributed to the presence of larger magnetic moments on Mn atoms than on Fe atoms.

The different contributions to the total energy in Eq. (2) differ in magnitude, and thus require differing degrees of accuracy. For this reason, we have separately checked the convergence of each of these contributions, with respect to the density of Brillouin zone (k-point) sampling. In all cases, a smearing of width 0.001 Ha was used to improve the convergence, except for the calculation of MAE, where a smaller smearing width of 0.0001 Ha was used.

IV. RESULTS

We first perform collinear magnetic calculations; these are useful not only because they might correspond to the magnetic ground state, but because the relative energies of FM and AFM states help to gauge the likelihood of obtaining non-collinear states such as spin spirals. We then go on to perform calculations on spin spirals with wavevectors $\mathbf{q}$ along high-symmetry directions of the Brillouin zone.

A. Collinear Magnetic Structures

We have considered two collinear magnetic configurations: (i) FM and (ii) row-wise AFM, for all four systems under study. These calculations were carried out using 132 $\mathbf{k}_\parallel$-points in the irreducible part of the surface Brillouin zone for FeAu$_2$/Ru(0001) and MnAu$_2$/Ru(0001), while for FeAu$_2$ and MnAu$_2$ monolayers 128 $\mathbf{k}_\parallel$-points were used in the irreducible Brillouin zone.

For the freestanding FeAu$_2$ monolayer, we find that the FM configuration is lower in energy than the AFM configuration, whereas for the freestanding MnAu$_2$ monolayer, the reverse is true. The energy difference between the two collinear magnetic structures considered, $\Delta E_{\rm AFM-FM}$, is 64 meV per Fe atom, for FeAu$_2$, and -70 meV per Mn atom for MnAu$_2$. However, when deposited on the Ru(0001) substrate, the ferromagnetic state is lower in energy for both the Fe and Mn surface alloys; the value of $\Delta E_{\rm AFM-FM}$ is found to be 62 meV per Fe atom for FeAu$_2$/Ru(0001), and 19 meV per Mn atom for MnAu$_2$/Ru(0001). The fact that the stability of the magnetic structure switches from being row-wise AFM for the freestanding monolayer, to FM for the deposited monolayer, for MnAu$_2$, is already an indication that the presence of the Ru substrate can play an important role in determining the magnetic properties of the system.

TABLE I. The magnetic moments on the various atoms in the alloy layer, and the top two layers of the substrate (where present), for the collinear ground state of the four systems studied. Ru(1) and Ru(2) atoms lie in the first and second layer, respectively, of the Ru substrate. See the text for the description of Ru(2)-I and Ru(2)-II.

Atom	Magnetic moments (μ_B)			
	FeAu$_2$/Ru	FeAu$_2$	MnAu$_2$/Ru	MnAu$_2$
Fe/Mn	2.88	3.2	3.75	± 4.14
Au	0.02	0.04	0.02	± 0.02
Ru(1)	0.00	-	-0.09	-
Ru(2)-I	-0.03	-	-0.02	-
Ru(2)-II	-0.11	-	-0.07	

In Table I, we have listed the magnetic moments for the different types of atoms in the row-wise AFM (for MnAu$_2$

monolayers) and FM (for the other three systems) configurations. As expected, the magnetic moments of the Fe and Mn atoms are higher in the freestanding monolayers, where the atoms have a lower coordination than when they are deposited on the Ru substrate. We find that the magnetic moments on the Au atoms tend to be aligned parallel to the X atoms, implying a ferromagnetic interaction between them, whereas, in general, the magnetic moments on the Ru atoms in the substrate are aligned opposite to those of the X atoms. Note that there are two inequivalent types of Ru atoms in the second layer of the substrate, labeled as Ru(2)-I and Ru(2)-II; these are situated directly below *X* and Au atoms, respectively.

B. Stability of the Surface Alloys

In order to check the stability of the surface alloys with respect to the phase segregated states [*X*/Ru(0001) and Au/Ru(0001)], we have obtained ΔH, the enthalpy of formation of the alloy, which is given by:

$$\Delta H = E_{X\mathrm{Au_2/Ru}} - \frac{1}{3}E_{X/\mathrm{Ru}} - \frac{2}{3}E_{\mathrm{Au/Ru}}, \qquad (6)$$

where E_C is the total energy of the system C. The above equation applies in the presence of the Ru substrate; for the freestanding monolayers, we of course use a similar equation involving freestanding systems with no Ru substrate present. Note that a positive/negative value of ΔH implies that the system is unstable/stable with respect to phase segregation.

To enable us to gauge the contribution of exchange interactions to ΔH, one can see how the enthalpy of formation changes when spin polarization is suppressed. Thus, the first two terms on the right-hand-side of Eq. (6) are computed in both the magnetic (M) and non-magnetic (NM) ground states; the corresponding values of ΔH are denoted as ΔH_{M} and ΔH_{NM}, respectively. Note that for these calculations the muffin-tin radius for the Mn atom has been taken to be 2.42 a.u. and 2.32 a.u. for the magnetic and non-magnetic calculations, respectively.

The magnetic ground states used in computing ΔH_{M} are as follows: for $FeAu_2$/Ru(0001) and $MnAu_2$/Ru(0001), they are the ferromagnetic state obtained in section IV.A. For Fe/Ru(0001), it is a 120° Néel state, which is lower in energy than the FM state by 58 meV per Fe atom.[19] For Mn/Ru(0001), it is the row-wise AFM state. For the freestanding $FeAu_2$ and $MnAu_2$ monolayers, it is the FM and row-wise AFM states, respectively, obtained in this study. For the freestanding Fe monolayer, it is a 2Q state,[29] and for a freestanding Mn monolayer it is the row-wise AFM state.

The values of ΔH_{M} and ΔH_{NM} are listed in Table II. Let us first focus on the values of ΔH_{NM}. These values are all positive, which implies that both the freestanding and the supported alloys are unstable with respect to the phase segregated states of *X*/Ru(0001) and Au/Ru(0001), when no magnetic interactions are present in the systems. However, if we focus on the values of ΔH_{M}, we find that the values become negative. This indicates that in the presence of magnetic interactions, all four surface alloys considered here become stable against phase segregation. Therefore, we conclude that magnetism plays a crucial role in the stability of these alloys.[14,15,30]

TABLE II. Listed below are the values of enthalpy of formation ΔH_{M} and ΔH_{NM} for the magnetic and non-magnetic systems, respectively. Note that here all the systems are taken to be in their respective collinear magnetic ground states.

System	Collinear magnetic state	ΔH_{NM} (meV/surface atom)	ΔH_{M}
$FeAu_2$/Ru(0001)	FM	12	-154
$MnAu_2$/Ru(0001)	FM	7	-177
$FeAu_2$	FM	31	-184
$MnAu_2$	Row-wise AFM	73	-333

In the phase-segregated situation, the magnetic moment in Fe/Ru(0001) is 2.75 μ_B per Fe atom;[19] this is increased to 2.88 μ_B in the surface alloy, where every Fe atom is surrounded by six Au atoms. This increase in magnetic moment and the magnetovolume effect provide the basic driving forces for the formation of the surface alloy. Similarly, the magnetic moment on the Mn atoms increases from 3.46 μ_B in Mn/Ru(0001) to 3.75 μ_B in $MnAu_2$/Ru(0001), which is why exchange interactions strongly favor the formation of the latter.

C. Spin Spiral Calculations for *X*Au_2/Ru(0001)

We now proceed to the question of primary interest for us, viz., whether the two supported systems, $FeAu_2$/Ru(0001) and $MnAu_2$/Ru(0001), exhibit a spin spiral ground state. While doing this, we have made use of the optimized geometry obtained for the collinear ferromagnetic state. In presenting these results, we have separated out each contribution to the energy [see Eq. (2)] of the spin spiral.

1. *Results for Heisenberg Exchange Energy* E_{HE}

As mentioned earlier, we have obtained $E_{\mathrm{HE}}(\lambda^{-1})$ using two possible approaches, the force theorem (FT), and self-consistently (SC). Let us first consider the results obtained using the former approach. In order to obtain converged results, we found that we need to use a very dense $\mathbf{k}_{\parallel}$-point mesh containing 6400 points in the full Brillouin zone. Since we know that the FT approach should be valid only for small perturbations, we perturb about a SC solution corresponding to the FM state (i.e., $\mathbf{q} = \mathbf{0}$), and restrict ourselves to regions of the Brillouin zone in the vicinity of the zone center. In particular, we consider $|\lambda^{-1}| \leq 0.32$ nm^{-1} along the [110] direction, and

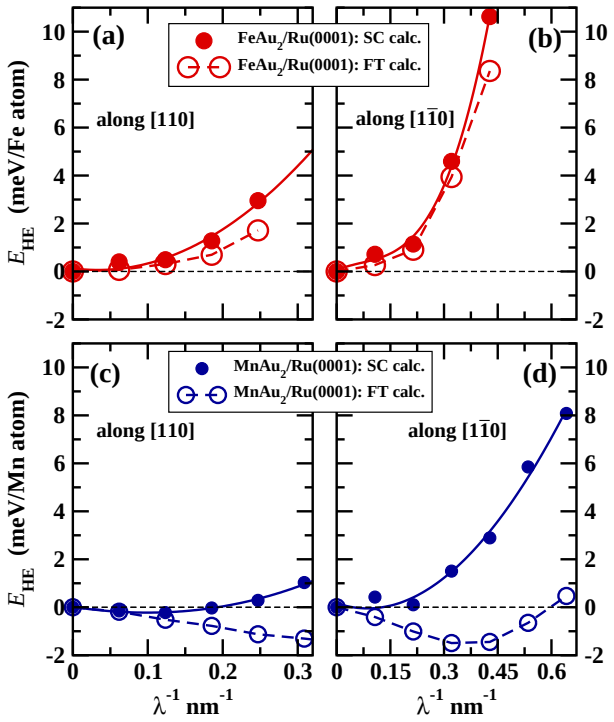

FIG. 2. (Color online) Dispersion of Heisenberg exchange energy $E_{\rm HE}$ for small λ^{-1}, for [(a) and (b)] $FeAu_2$/Ru(0001) and [(c) and (d)] $MnAu_2$/Ru(0001), along high-symmetry directions in the Brillouin zone. The open circles are the results from the force theorem (FT) calculations. The filled circles are results from the self-consistent (SC) calculations and correspond to the zoomed-in regions of the top panel of Fig. 3.

$|\lambda^{-1}| \leq 0.75$ nm^{-1} along [1$\bar{1}$0]. Our results are shown by the open circles in Fig. 2. [Note that as the relation $E_{\rm HE}(-\lambda^{-1}) = E_{\rm HE}(\lambda^{-1})$ holds for both systems, we have only shown the results for $\lambda^{-1} > 0$]. Interestingly, we find that for $MnAu_2$/Ru(0001), the graphs suggest that even with Heisenberg exchange interactions alone, a spin spiral state would be favored over the ferromagnetic state. However, for $FeAu_2$/Ru(0001), the ground state in this approximation remains the FM state.

Next, we proceed to verify these FT results by performing more accurate SC calculations. For these, we found that it sufficed to use 512 and 800 $\mathbf{k}_{\|}$-points when sampling the irreducible Brillouin zones for $FeAu_2$/Ru(0001) and $MnAu_2$/Ru(0001), respectively. These results are shown by the filled circles in Fig. 2. Somewhat surprisingly, the results obtained now are quite different, especially for $MnAu_2$/Ru(0001). The difference in energy between a spin spiral state and the FM state is now considerably reduced.

This suggests that results using the FT approach cannot always be trusted, and the force theorem must be used with considerable caution. This point is discussed further in the Appendix to this paper.

We now go on to use the SC approach to compute $E_{\rm HE}$ throughout the Brillouin zone, along high-symmetry directions. This, along with results for the variation of magnetic moments, are shown in Fig. 3. In this figure, $\overline{\Gamma \rm K}$ and $\overline{\Gamma \rm M}$ lie within the first Brillouin zone, while $\overline{\rm KM'}$ belongs to the second Brillouin zone. On examining this figure, we see that for $FeAu_2$/Ru(0001), the lowest value of $E_{\rm HE}$ is at the $\overline{\Gamma}$ point (see the top two panels of Fig. 3). In contrast, for $MnAu_2$/Ru(0001), the lowest value of $E_{\rm HE}$ corresponds to a spin spiral with $\lambda^{-1} = 0.12$ nm^{-1} along the $\overline{\Gamma \rm M}$ direction. This is more evident from Fig. 2(c) (see the solid line and filled circles). Note however that: (i) the difference in $E_{\rm HE}$ between the FM state and the spin spiral state is small, and (ii) to obtain the final result for ground state magnetic structure, we have yet to add the other two contributions $E_{\rm DM}$ and $K_{\rm avg}$, to $E_{\rm HE}$.

The magnetic moments of the X atoms, M_X, (shown by the stars in the middle panel of Fig. 3) vary only slightly as $\mathbf{q}$ changes. The induced moments on the Au, Ru(2)-I and Ru(2)-II atoms can be either positive (ferromagnetically aligned) or negative (antiferromagnetically aligned), depending on the value of $\mathbf{q}$; however the magnitude of these induced moments is small.

2. *Results for Dzyaloshinskii-Moriya Energy $E_{\rm DM}$*

We next calculate $E_{\rm DM}(\lambda^{-1})$ for $FeAu_2$/Ru(0001) and $MnAu_2$/Ru(0001). For all the spin spirals considered by us, the relation $E_{\rm DM}(-\lambda^{-1}) = -E_{\rm DM}(\lambda^{-1})$ holds, where positive and negative values of λ^{-1} correspond to right-rotating and left-rotating spirals, respectively. We have obtained the different components of $\mathbf{D}$ by varying $\mathbf{q}$ along the [110] direction, with -0.25 nm$^{-1} < \lambda^{-1} < 0.25$ nm^{-1}, and along the [1$\bar{1}$0] direction with -0.42 nm$^{-1} < \lambda^{-1} < 0.42$ nm^{-1}. The calculations were performed using 6400 $\mathbf{k}_{\|}$-points in the full surface Brillouin zone. Our results are presented in Fig. 4. For both $FeAu_2$/Ru(0001) and $MnAu_2$/Ru(0001), we have found that $E_{\rm DM}$ always favors left-rotating spirals, we have therefore shown only the negative λ^{-1} region in this figure.

Our results for $E_{\rm DM}(\lambda^{-1})$ for $FeAu_2$/Ru(0001) and $MnAu_2$/Ru(0001) are shown by the open and filled squares, respectively, in Fig. 4. We find that the magnitude of $E_{\rm DM}$ is significantly larger for $FeAu_2$/Ru(0001) than it is for $MnAu_2$/Ru(0001) (the reason for this will be discussed below); note that this was however also true of the magnitude of $E_{\rm HE}$, and that for negative λ^{-1} these two terms have opposite sign, leading in both cases to a similar compensation of energies. Further, $E_{\rm DM}(\lambda^{-1})$ is found to be linear for $FeAu_2$/Ru(0001), along both the [110] and [1$\bar{1}$0] directions, for the range of λ^{-1} considered here. However, we can see that this is clearly not true for $MnAu_2$/Ru(0001), where $E_{\rm DM}(\lambda^{-1})$ is found to deviate from linear behavior for $\lambda^{-1} \gtrsim -0.19$ nm^{-1}, along both directions. In the region where $E_{\rm DM}$ varies linearly with λ^{-1}, we fitted our data to straight lines (see the black lines in Fig. 4), so as to obtain the components of $\mathbf{D}$ along different directions. We obtain D_x and D_y by fitting along

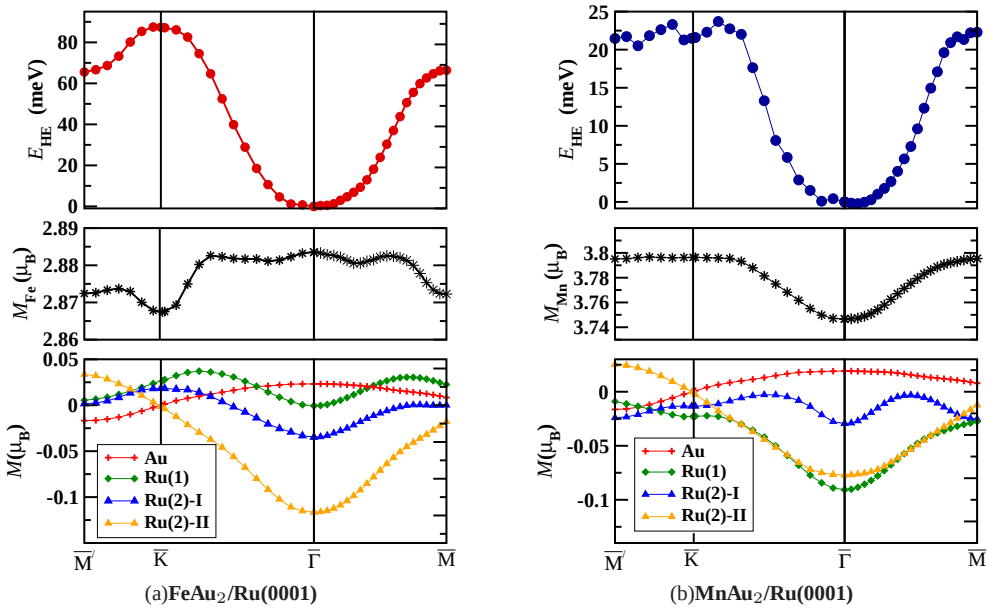

FIG. 3. (Color online) Results from SC calculations for variation of Heisenberg exchange energy $E_{\rm HE}$, and magnetic moments M on the different atoms, along high symmetry directions of the surface Brillouin zone, for (a) $FeAu_2$/Ru(0001) and (b) $MnAu_2$/Ru(0001). $E_{\rm HE}$ is given in meV per X atom, and M is given in μ_B per atom. See the text for the convention used in labeling atoms.

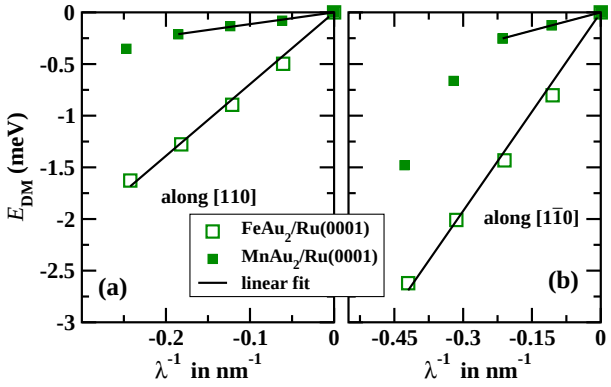

FIG. 4. (Color online) $E_{\rm DM}$, contribution from the Dzyaloshinskii-Moriya interaction, to the total energy along (a) [110] and (b) [1$\bar{1}$0] for $FeAu_2$/Ru(0001) and $MnAu_2$/Ru(0001).

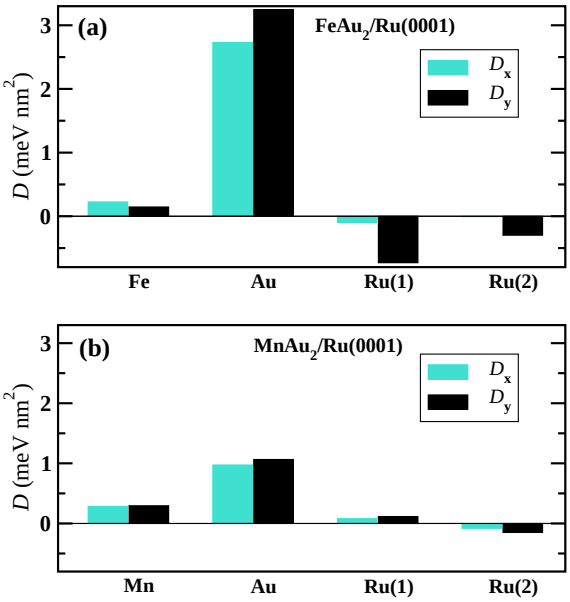

FIG. 5. (Color online) Atom-wise contributions to non-zero components of $\mathbf{D}$ for (a) $FeAu_2$/Ru(0001) and (b) $MnAu_2$/Ru(0001). Along [110] $D_y \neq 0 = D_x$, while along [1$\bar{1}$0] $D_x \neq 0 = D_y$. X, Au and Ru(n) indicate the magnetic atom (Fe or Mn), Au atom and n-th layer Ru atoms, respectively, where n=1 and 2.

the [1$\bar{1}$0] and [110] directions, respectively; we find that the D_z component always vanishes. For $FeAu_2$/Ru(0001), we obtain the values of D_x and D_y to be 6.40 and 6.94 meV nm^2, respectively, whereas for $MnAu_2$/Ru(0001), the values of D_x and D_y are found to be 1.17 and 1.12 meV nm^2, respectively.

We have also extracted the contributions to $\mathbf{D}$ that arise from each kind of atom,[26] focusing on the X, Au, Ru(1) and Ru(2) atoms, as the DM interaction is expected to be significant only near the surface. [Note that here, by the contribution of the Ru(2) atoms we mean the average contribution of the Ru(2)-I and the Ru(2)-II atoms.] These atom-wise contributions are depicted graphically in Fig. 5. It is interesting to note that for both $FeAu_2$/Ru(0001) and $MnAu_2$/Ru(0001), the largest (positive) contributions arise from the Au atoms. The contributions coming from the X atoms also always enhance $\mathbf{D}$, but the magnitude is much smaller compared to those from the Au atoms. The Ru(1) and Ru(2) atoms have contributions reducing $\mathbf{D}$, except

for $MnAu_2$/Ru(0001), where Ru(1) contributes additively. There are two possible ways in which two magnetic atoms can interact through the DM mechanism, either directly, or involving a third, "non-magnetic" atom.[31] In our case, this third atom could be either Ru or Au. Our results suggest that it is this latter, three-site mechanism that is dominant in our case. The much larger contribution from Au atoms is in accordance with the large spin-orbit coupling in Au and the strong buckling of the overlayer. The larger buckling in $FeAu_2$/Ru(0001) than $MnAu_2$/Ru(0001) also leads to a stronger contribution to **D**.

3. *Results for Magnetic Anisotropy Energy K*

The third contribution to the energies of spin spirals on $FeAu_2$/Ru(0001) and $MnAu_2$/Ru(0001) consists of the magnetic anisotropy energy K. For both these systems, we have calculated the energy barriers for a rotation of the magnetic moment in the xz and yz planes, which are given respectively by:

$$K^{110} = E(\theta = \theta_1^{\rm hard}, \varphi = 0) - E(\theta = \theta_1^{\rm easy}, \varphi = 0), \tag{7}$$

$$K^{1\bar{1}0} = E(\theta = \theta_2^{\rm hard}, \varphi = \tfrac{\pi}{2}) - E(\theta = \theta_2^{\rm easy}, \varphi = \tfrac{\pi}{2}), \tag{8}$$

where E is the energy, obtained including spin-orbit interactions, and the moments on the X atoms are constrained to point along the direction specified by the angles (θ, φ); the polar angle θ is measured from the surface normal and the azimuthal angle φ is measured from the x-axis [see Fig. 1(a)]. The easy and hard axes for the two rotations are specified by the angles $\theta_i^{\rm easy}$ and $\theta_i^{\rm hard}$. K has two contributions: $K_{\rm SO}$ and $K_{\rm dip}$, which arise from spin-orbit interactions, and magnetic dipolar interactions, respectively.

Let us first consider $K_{\rm SO}$, which can be calculated in two possible ways: either self-consistently (SC) or by using the force theorem (FT). To check the applicability of the FT for the calculation of the MAE of the systems considered here, we first compute as a test the quantity $K_{\rm test} = E(\theta = \frac{\pi}{2}, \varphi = 0) - E(\theta = 0, \varphi = 0)$, using both approaches. The number of k-points required for a converged SC calculation is 256 in the full Brillouin zone, while 4096 k-points are needed for the FT calculations. For $FeAu_2$/Ru(0001), we obtain $K_{\rm test}$ = 1.14 and 0.93 meV per Fe atom, from the FT and SC approaches, respectively; the corresponding values for $MnAu_2$/Ru(0001) are 0.18 meV and 0.19 meV per Mn atom. Based upon this, we conclude that results for $K_{\rm SO}$ using the two approaches are likely to agree to the desired degree of accuracy. Henceforth, we have used the FT to calculate all the values of K reported in this section.

We now proceed to vary θ, keeping φ fixed at a constant value φ_c, which is equal to either 0 or $\frac{\pi}{2}$, when determining K along the [110] and [$1\bar{1}0$] directions, respectively. We define

$$E_\perp(\theta, \varphi_c) = E^{\rm SO}(\theta, \varphi_c) - E^{\rm SO}(0, \varphi_c). \tag{9}$$

In Fig. 6(a), we have plotted our results for $E_\perp$ for $FeAu_2$/Ru(0001) and $MnAu_2$/Ru(0001), with $\varphi_c = 0$. The results for the two systems are quite different. For $FeAu_2$/Ru(0001), the highest value of $E_\perp$ occurs for $\theta = 0$, and the lowest value for $\theta = \frac{\pi}{2}$, whereas for $MnAu_2$/Ru(0001), the angles corresponding to the highest and lowest values of $E_\perp$ are reversed. This suggests that (assuming that the contribution from dipolar interactions is small; this remains to be verified below) the position of the hard and easy axes is interchanged in the two systems studied here. It is also interesting to note that K is significantly higher for $FeAu_2$/Ru(0001) than for $MnAu_2$/Ru(0001).

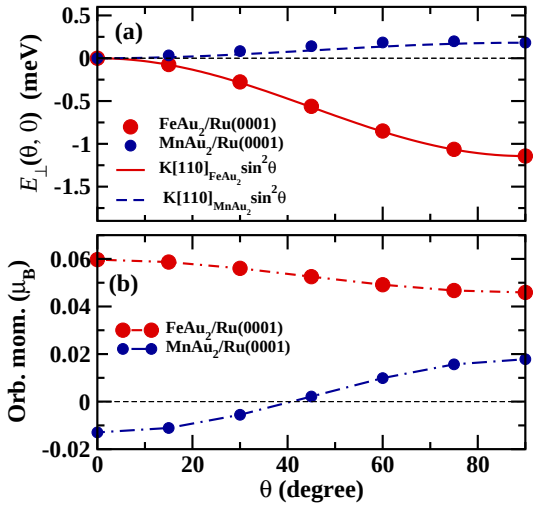

FIG. 6. (Color online) The variation of (a) $E_\perp(\theta, \varphi_c = 0)$ and (b) orbital moment of the X atom as a function of the polar angle θ for $FeAu_2$/Ru(0001) and $MnAu_2$/Ru(0001). The easy axis lies along the direction of minimum $E_\perp(\theta, \varphi_c = 0)$.

TABLE III. Results for magnetic anisotropy energy K, along with $K_{\rm SO}$ and $K_{\rm dip}$, the contribution due to spin-orbit coupling and magnetic dipole-dipole interaction, respectively, along two high-symmetry directions, for XAu$_2$/Ru(0001).

X	direction	$K_{\rm SO}$	$K_{\rm dip}$	K
		(meV per X atom)		
Fe	[110]	1.14	0.04	1.18
	[$1\bar{1}0$]	1.18	0.04	1.22
Mn	[110]	0.18	−0.06	0.12
	[$1\bar{1}0$]	0.14	−0.06	0.08

We have also shown, in Fig. 6(b), how the orbital moment per X atom changes as θ is varied. One observes a sinusoidal variation, though the amplitude of variation is

small. We find that, for both systems, the highest and lowest values of orbital moment occur when the magnetization is along the hard-axis and the easy-axis, respectively. Note that this contradicts with the prediction of Bruno.[32] The prediction is based on the assumption that the majority and minority d-bands are well separated by the exchange interaction; though this is true for the X atoms, for the Ru atoms this assumption does not hold true.

Next, we consider $K_{\rm dip}$, which arises from the magnetostatic interaction between the magnetic moments. We find that the contributions to K from dipolar interactions are significantly smaller than those from the spin-orbit interaction, especially for $FeAu_2$/Ru(0001). Our results for $K_{\rm dip}$ are listed in the fourth column of Table III. The negative sign of $K_{\rm dip}$ for the Mn alloy indicates that the easy axis is out-of-plane here, while dipolar interactions always favor an in-plane axis for ferromagnetic configurations.

Finally, the total value of K is obtained by adding $K_{\rm SO}$ and $K_{\rm dip}$ (see the last column in Table III). We also obtain $K_{\rm avg}$, the average value of K in the (110) and $(1\bar{1}0)$ planes [see Eq. (2)]; in all the cases studied here, $K_{\rm avg} = K/2$. We find that the easy axis lies in-plane for $FeAu_2$/Ru(0001), but out-of-plane for $MnAu_2$/Ru(0001).

4. *Results for $E_{\rm total}$*

Having obtained the values of $E_{\rm HE}$, $E_{\rm DM}$ and $K_{\rm avg}$, we are now finally in a position to calculate the total energy $E_{\rm total}$ for $FeAu_2$/Ru(0001) and $MnAu_2$/Ru(0001). In Fig. 7, the values of $E_{\rm HE}$ and $E_{\rm DM}$ are shown by circles and squares, and the value of $K_{\rm avg}$ is shown by dashed lines. The final values $E_{\rm total}$, obtained by adding these three terms, are shown by the stars and the solid black curves fit to them.

For $FeAu_2$/Ru(0001), we find that along the [110] direction, the most energetically favorable state is a left-rotating spin spiral with $\lambda^{-1} = -0.14$ nm^{-1}, this is lower in energy than the FM state by 0.06 meV per Fe atom [see Fig. 7(a)]. Along $[1\bar{1}0]$, a spin spiral of $\lambda^{-1} = -0.15$ nm^{-1} becomes lower in energy than the FM state by 0.17 meV per Fe atom [see Fig. 7(b)]. This latter spin spiral, with a wavelength of 6.7 nm, is the lowest-energy magnetic ground state for $FeAu_2$/Ru(0001). However, it is only very slightly lower in energy than the FM state.

Similarly, the lower two panels of Fig. 7 show the various contributions to the energies of spin spirals on $MnAu_2$/Ru(0001). We see that a left-rotating spin spiral with $\lambda^{-1} = -0.12$ nm^{-1} along [110] is lower in energy than the FM state by 0.28 meV per Mn atom, while a left-rotating spin spiral with $\lambda^{-1} = -0.08$ nm^{-1} along $[1\bar{1}0]$ is lower in energy than the FM state by 0.17 meV per Mn atom. Of these, the former, with a wavelength of 8.5 nm, is the magnetic ground state.

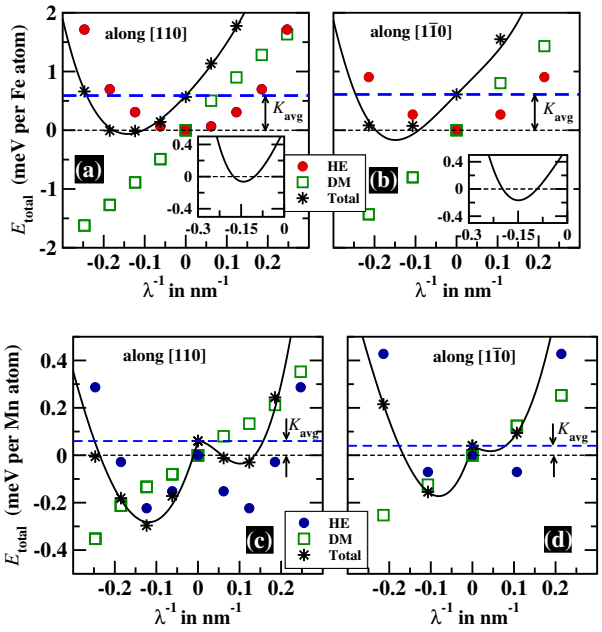

FIG. 7. (Color online) Variation of total energy ($E_{\rm total}$) as a function of λ^{-1} for [(a) and (b)] $FeAu_2$/Ru(0001) and [(c) and (d)] $MnAu_2$/Ru(0001) along [110] and $[1\bar{1}0]$. The insets in (a) and (b) are zoomed in areas using the same scale as in (c) and (d).

D. Comparison with Freestanding Alloy Monolayers of XAu_2

In order to gauge what effect the Ru substrate has, we now repeat the previous calculations, but for freestanding XAu_2 alloy monolayer systems, i.e., in the absence of the Ru substrate. As before, we present separately the contributions to the total energy from each term in Eq. (2).

1. *Results for Heisenberg Exchange Energy $E_{\rm HE}$*

We have calculated $E_{\rm HE}$ for freestanding $FeAu_2$ and $MnAu_2$ monolayers. From the already presented calculations on collinear magnetic structures (see Section IV.A above), we have seen that both $FeAu_2$ and $MnAu_2$ freestanding monolayers remain flat upon relaxation, i.e., no buckling is observed. We now restrict ourselves to calculating $E_{\rm HE}$ self-consistently (SC) for flat freestanding monolayers (see also the Appendix). We find that it is adequate to use 78 k-points in the irreducible Brillouin zone.

Fig. 8 shows our results for $E_{\rm HE}$ along high-symmetry directions of the Brillouin zone for both $FeAu_2$ and $MnAu_2$ freestanding monolayers. We find that the lowest $E_{\rm HE}$ states are FM for $FeAu_2$ – see the large (red) dots – and row-wise AFM for $MnAu_2$ – see the small (blue) dots. Thus, for the freestanding alloy monolayers, we find that the collinear magnetic states are lower in energy than the spin spiral states. Note that for flat monolayers, $E_{\rm DM}$ is identically zero. So, upon going from freestanding alloy

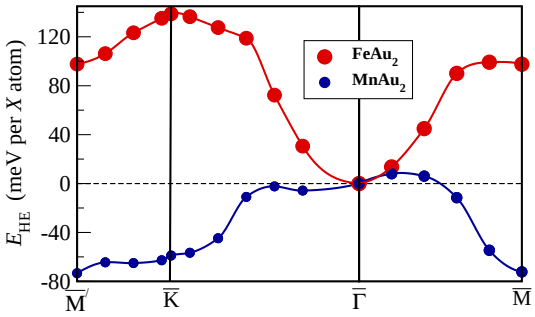

FIG. 8. (Color online) Energy dispersion $E_{\rm HE}$ for freestanding monolayers of $FeAu_2$ [shown by gray (red) dots] and $MnAu_2$ [shown by dark (blue) dots]. The ground state magnetic structure for $FeAu_2$ is ferromagnetic (minimum at $\overline{\Gamma}$), whereas that for $MnAu_2$ is row-wise antiferromagnetic (minimum at $\overline{\rm M}$).

monolayers to surface alloys on Ru(0001), the magnetic ground state changes from FM to a spin spiral state in the case of $FeAu_2$/Ru(0001), while for $MnAu_2$/Ru(0001), the ground state changes from a row-wise AFM state to a spin spiral state.

2. *Results for Dzyaloshinskii-Moriya Energy* $E_{\rm DM}$

Though the freestanding $X\mathrm{Au}_2$ monolayers do not show any buckling, in order be able to compare the asymmetric exchange coupling between the X and Au atoms with and without the substrate, we have obtained the value of $\mathbf{D}$ as a function of the buckling parameter $d_{\rm b}$ of the freestanding monolayers of $X\mathrm{Au}_2$. We have taken $d_{\rm b}$ to be 0.5, 1.0 and 1.5 Å. Further, in order to better enable a comparison with the corresponding systems on the Ru substrate, we have also considered $d_{\rm b}$ to be 0.38 Å (for the $FeAu_2$ monolayer) and 0.22 Å (for the $MnAu_2$ monolayer); these values correspond to the values of $d_{\rm b}$ for the overlayer in the $X\mathrm{Au}_2$/Ru(0001) systems.

In Fig. 9, we have plotted our results for D_x and D_y, as a function of buckling parameter $d_{\rm b}$, for freestanding $FeAu_2$ and $MnAu_2$ monolayers; the component D_z vanishes in all the cases considered here. For purposes of comparison, the values of D_x and D_y for the corresponding $X\mathrm{Au}_2$/Ru(0001) systems are shown by dashed and dotted lines, respectively. We find that for $FeAu_2$ monolayers, the values of both D_x and D_y at $d_{\rm b} = 0.38$ Å are much smaller than the corresponding values for $FeAu_2$/Ru(0001). In contrast, for $MnAu_2$ monolayers, the values of D_x and D_y are similar to the values for $MnAu_2$/Ru(0001). It is therefore difficult to reach any general conclusions about the effect of the Ru substrate; it is apparently system-dependent, since the magnetic interactions between the Fe and Ru atoms differ from those between the Mn and Ru atoms. We also observe that for the alloy monolayers, the values of D_x and D_y can differ a lot, whereas the values are almost the same for the $X\mathrm{Au}_2$/Ru(0001) systems.

For $FeAu_2$/Ru(0001) the largest values of D_x and D_y occur for $d_{\rm b} = 0.5$ Å, while for $MnAu_2$/Ru(0001), we find the values are the largest at $d_{\rm b} = 1.0$ Å. We obseve that two competing effects determine the magnitude of $\mathbf{D}$: (i) a geometrical effect that enhances its value with increasing buckling and (ii) the influence of the distance between X and Au, that decreases $\mathbf{D}$ if the X-Au distance is too large. This is in line with the model of Levy and Fert[31] for the DM interaction.

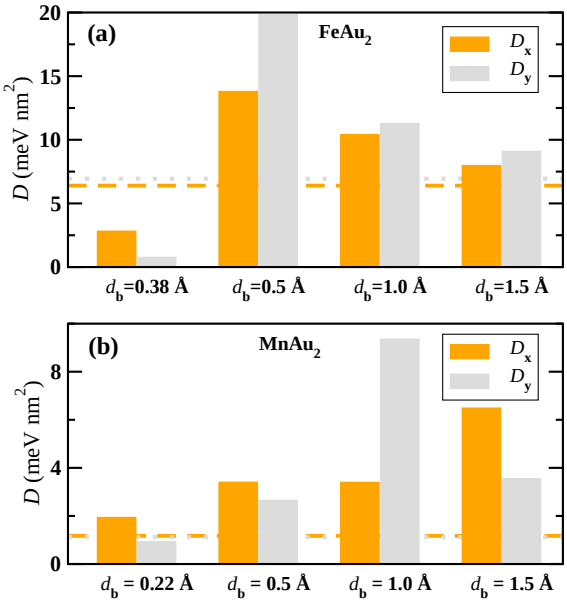

FIG. 9. (Color online) The variation of D_x and D_y as a function of overlayer buckling $d_{\rm b}$ for freestanding monolayers of (a) $FeAu_2$ and (b) $MnAu_2$. Along [110] $D_y \neq 0 = D_x$, while along [1$\overline{1}$0] $D_x \neq 0 = D_y$. The dashed and dotted lines correspond to the values of D_x and D_y, respectively, in the case of $FeAu_2$/Ru(0001) and $MnAu_2$/Ru(0001). Note that the y-axis scale is different in (a) and (b).

3. *Results for Magnetic Anisotropy Energy* K

We have calculated the value of the magnetic anisotropy energy K for freestanding monolayers of $X\mathrm{Au}_2$. Test calculations show that results obtained using the FT and SC methods are comparable. We therefore continue by using the FT. We find that it suffices to use 4096 and 6400 $\mathbf{k}_{\parallel}$-points in the Brillouin zone for the calculation of $K_{\rm SO}$ for the $FeAu_2$ and $MnAu_2$ monolayers, respectively.

In Fig. 10(a), we have plotted our results for $E_\perp(\theta, \varphi_c = 0)$ vs. θ. The small (red) dots and large (blue) dots show the results for freestanding $FeAu_2$ and $MnAu_2$ monolayers, respectively. We have fitted $E_\perp$ to $\sin^2\theta$ (solid line). The positions of the minimum and maximum values of $E_\perp$ are seen to be the same as in the presence of the Ru(0001) substrate, and are again opposite for the two different X. However, the values of $K_{\rm SO}$ are found to have become significantly larger in the absence of the Ru substrate.

From Fig. 10(b), we see that the value of the orbital mo-

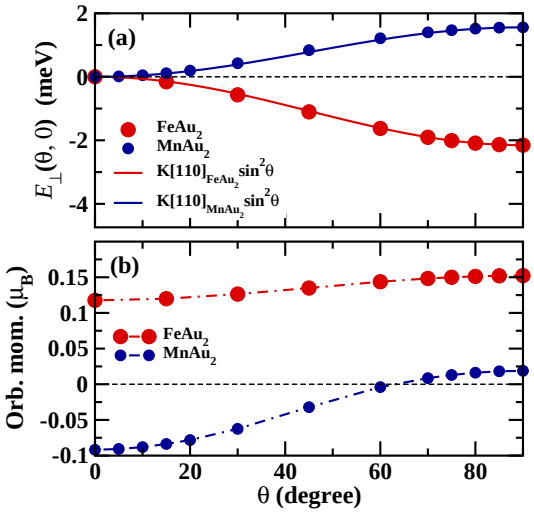

FIG. 10. (Color online) The variation of (a) $E_\perp(\theta, \varphi_c = 0)$ and (b) orbital moment of the X atom as a function of the polar angle θ for $FeAu_2$ and $MnAu_2$ freestanding monolayers. The easy axis lies along the direction of minimum $E_\perp(\theta, \varphi_c = 0)$.

TABLE IV. Values of $K_{\rm SO}$ and $K_{\rm dip}$, the contributions to MAE due to spin-orbit coupling and dipole-dipole interaction, respectively, for freestanding XAu$_2$ monolayers. μ_z and μ_x are the orbital moments when magnetization points along z- and x-axis, respectively.

X	$K_{\rm SO}$	$K_{\rm dip}$	μ_z	μ_x
	(meV per X atom)		(μ_B)	
Fe	2.1	0.05	0.12	0.15
Mn	1.8	−0.08	−0.09	0.02

ment per X atom is the highest along the easy-axis for the freestanding monolayers of $FeAu_2$ and $MnAu_2$. This behavior differs from the trend seen in the XAu$_2$/Ru(0001) systems, though it is consistent with the prediction of Bruno.[32] The values of orbital moments are larger for the freestanding monolayers than the corresponding values on the deposited monolayers. This quenching of the orbital moments is an effect of the crystal field of the substrate.

We find that the value of $K_{\rm SO}$ does not differ appreciably in the [110] and $[1\bar{1}0]$ directions; it is 2.1 meV per Fe atom for the $FeAu_2$ monolayer, and 1.8 meV per Mn atom for the $MnAu_2$ monolayers. Note that the direction of the easy axis differs in the two cases, for the former it is in-plane, while for the latter it is out-of-plane.

Next, we have obtained the values of $K_{\rm dip}$ for the freestanding alloy monolayers of XAu$_2$; once again we do not find an appreciable difference between our results for the [110] and $[1\bar{1}0]$ directions. For $FeAu_2$ monolayers the value of $K_{\rm dip}$ is 0.05 meV per Fe atom, compared to the value of 0.04 meV per Fe atom for $FeAu_2$/Ru(0001) (see Table III). The values of $K_{\rm dip}$ for $MnAu_2$ and $MnAu_2$/Ru(0001) are -0.08 and -0.06 meV per Mn atom, respectively. The slightly higher values of $K_{\rm dip}$ for the freestanding monolayers arise from the higher values of the magnetic moments.

V. DISCUSSION

A. Stability of the Surface Alloys

In Table II we had determined the stability of the surface alloys $FeAu_2$/Ru(0001) and $MnAu_2$/Ru(0001), with respect to the phase-segregated elemental monolayers on Ru(0001). We had also examined the miscibility of the corresponding freestanding monolayers. In this table, however, we had only considered collinear magnetic structures for the four surface alloy systems. We have now found that the magnetic ground state for the two supported surface alloy systems is not the ferromagnetic state but a spin spiral; however, the energy difference between these two is small. Therefore, the values in Table II do not change appreciably upon considering non-collinear configurations for the mixed phases. For $FeAu_2$/Ru(0001), ΔH is further lowered by only 0.04% further, while for $MnAu_2$/Ru(0001), ΔH is further decreased by only 0.05%.

B. Relative Contributions of Different Terms to $E_{\rm total}$

It is interesting to note that the primary reason for obtaining the spin spiral ground states is different for $FeAu_2$/Ru(0001) and $MnAu_2$/Ru(0001). By examining Fig. 7, we see that for $FeAu_2$/Ru(0001), it is the DM interaction that is chiefly responsible for stabilizing the spin spiral ground state over the FM state. In contrast, for $MnAu_2$/Ru(0001) the predominant role is played by the Heisenberg exchange interaction. One reason why the DM interaction is stronger in the case of $FeAu_2$/Ru(0001) is the larger value of the buckling parameter $d_{\rm b}$ in this system. From comparison to the unsupported alloys it can be seen that, in addition, also the chemical nature of the magnetic element and its modification by the Ru substrate by bonding (charge transfer) have an important influence on the strength of this interaction. The propensity of Heisenberg exchange to favor spin spirals is indicated by a small value of $\Delta E_{\rm AFM-FM}$; we have already seen above that this quantity is smaller for $MnAu_2$/Ru(0001) than $FeAu_2$/Ru(0001).

C. Role of Au

It was mentioned earlier that Fe/Ru(0001) shows a 120° Néel structure[19] and Mn/Ru(0001) shows a row-wise AFM structure.[20] In this study, we see that the magnetic interaction changes in these systems, due to the presence of Au in the overlayer, and the systems are driven toward a spin spiral ground state in $FeAu_2$/Ru(0001) and $MnAu_2$/Ru(0001), due to complex magnetic interactions.

From Section IV.C2, we also see that due to the large spin-orbit coupling constant of Au atoms, the DM interaction mainly acts via these atoms, rather than the Ru atoms. On the other hand, it is the Ru substrate that makes the Au contribution very different in the Fe and Mn systems. The large additive contribution of the Au atoms toward the DM parameter thus helps to lower the energy of a spin spiral compared to the FM state, especially in the case of $FeAu_2$/Ru(0001).

VI. SUMMARY

In summary, we have performed *ab initio* density functional theory calculations to obtain the magnetic ground states of two surface alloys: $FeAu_2$/Ru(0001) and $MnAu_2$/Ru(0001). By considering both collinear and non-collinear magnetic structures, we have found that the magnetic ground state for both systems corresponds to a left-rotating spin spiral. For the Fe system the spiral propagates along the $[110]$ direction with a period of 6.7 nm, while in the Mn alloy it is along $[1\bar{1}0]$ and has a period of 8.5 nm. In the former case, the spin spiral is stabilized by the Dzyaloshinskii-Moriya interaction, whereas in the latter case it is primarily stabilized by the Heisenberg exchange interaction. These results show that magnetic surface alloys constitute a new class of systems that can be explored for the existence of spin spirals. However, in the two particular systems considered in this work, the spin spiral states are only slightly lower in energy than the ferromagnetic state, by 0.17 and 0.28 meV per Fe and Mn atom, respectively.

We have seen that the strength of the DM interactions is very sensitive to the buckling of the overlayer. Of the two surface alloy systems considered in this study, $FeAu_2$/Ru(0001) has a buckling that is almost twice as large as that observed in $MnAu_2$/Ru(0001), and the values of D_x and D_y are larger by a factor of $\sim$6–7. For a monolayer on a substrate, the buckling is fixed, being determined by the size mismatch between the overlayer and substrate atoms. However, when one considers surface alloys of the type AB/C, as in this study, one has more parameters to play with, since the buckling depends not only on the size difference between the overlayer atoms and the substrate, but also on the size difference between the two overlayer constituents A and B. One therefore has the ability to tune the buckling, and thus the strength of the DM interaction, over a wider range; this can be made use of as a way of further stabilizing spin spirals.

We also find that $FeAu_2$/Ru(0001) has a significantly high magnetic anisotropy energy, of the order of 1 meV per Fe atom, with an in-plane easy-axis. On the other hand, $MnAu_2$/Ru(0001) has a magnetic anisotropy energy that is smaller by an order of magnitude, and an out-of-plane easy axis. Upon comparing these values of the MAE with those obtained for the corresponding freestanding monolayers, we find that for both the systems, the presence of the substrate does not alter the direction of the easy-axis, but reduces the magnitude of the MAE considerably.

It has been shown in earlier work that magnetic interactions are primarily responsible for stabilizing the $FeAu_2$/Ru(0001) surface alloy against phase-segregation.[15] In addition to confirming these results, we now find that this is also true for the $MnAu_2$/Ru(0001) system, as well as the corresponding freestanding monolayers. For FeAu alloys on Ru(0001), it has been concluded that an important role is played by ferromagnetically polarized substrate Ru atoms.[30] However, these are of course absent in the freestanding alloy monolayers, while even in our two supported alloy systems, we find that the substrate Ru atoms are primarily spin polarized antiparallel to the overlayer Mn atoms. The main driving force for alloy formation is that by forming an alloy structure where the "magnetic" (Fe or Mn) atom is surrounded in the overlayer by Au atoms, it can raise its magnetic moment, and thus significantly lower the exchange energy. This effect is sufficiently strong to flip the enthalpy of formation from being positive to being negative.

By comparing with the corresponding freestanding alloy monolayers, we find that the presence of the Ru substrate plays a crucial role in determining the magnetic properties of the surface alloy systems and Au atoms in the overlayer promote chirality in these systems.

Our results underline the need for considerable caution when applying the magnetic force theorem in calculations of magnetic structures, when small energy scales are involved.

Most importantly, we wish to underline that our work shows that bimetallic magnetic surface alloy systems of the type AB/C, such as those studied here, allow one to play with and tune the Dzyaloshinskii-Moriya interaction, thus allowing one to access novel magnetic structures such as spin spirals. Such surface alloys, which contain a heavy atom in the topmost layer, give one a way to the DM interaction via the structure, in contrast to A/B thin-film systems. This leads to the possibility of manipulating the spin spiral via electric fields or adsorbates.

Appendix A: Applicability of the Force Theorem

In section IV.C1, we showed that the force theorem failed to yield an accurate value for δE_{HE}, the difference in energy from Heisenberg exchange interactions, between two spin spirals of slightly different wavelength, especially for $MnAu_2$/Ru(0001). Here, we discuss this issue further.

We first consider conical spin spirals, where the magnetic moments are not constrained to lie in a plane, but precess around the axis of rotation, making an angle α with it. Note that for planar spin spirals, $\alpha = \frac{\pi}{2}$. The energy difference $\delta E_{\mathrm{HE}}(\alpha)$ between two spin spirals with wavevectors $\mathbf{q}_1$ and $\mathbf{q}_2$ can be written as:[33]

$$\delta E_{\rm HE}(\alpha) = E^{\mathbf{q}_1}_{\rm HE}(\alpha) - E^{\mathbf{q}_2}_{\rm HE}(\alpha), \quad \text{(A1)}$$

$$\simeq \sin^2\alpha\,(E^{\mathbf{q}_1}_{\rm HE}(\frac{\pi}{2}) - E^{\mathbf{q}_2}_{\rm HE}(\frac{\pi}{2})),$$

$$\equiv \sin^2\alpha\,\delta E_{\rm HE}(\frac{\pi}{2}), \quad \text{(A2)}$$

where the approximation holds for a small difference between $\mathbf{q}_1$ and $\mathbf{q}_2$, and does not depend on the method of calculation (FT or SC). For our calculations we have taken $|\mathbf{q}_1|$ and $|\mathbf{q}_2|$ to be 0 and 3.3 nm^{-1}, respectively, for $MnAu_2$/Ru(0001), and 8.8 and 11 nm^{-1}, respectively, for freestanding $MnAu_2$, along the [110] direction.

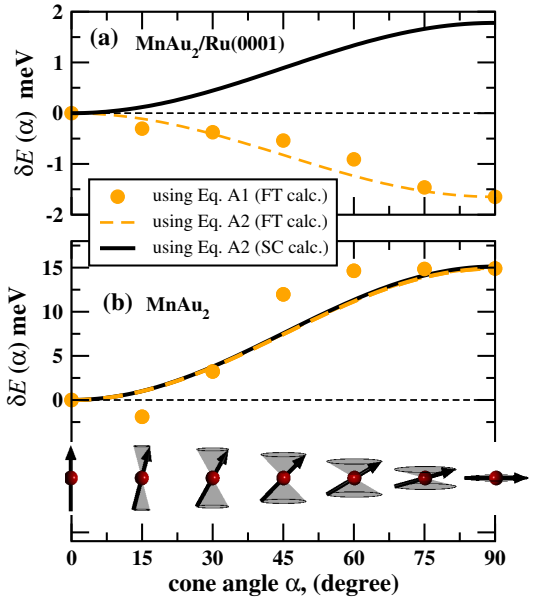

FIG. 11. (Color online) The variation of $\delta E_{\rm HE}(\alpha)$ as a function of the cone angle α for (a) $MnAu_2$/Ru(0001) and (b) $MnAu_2$ freestanding monolayers. The gray (orange online) dots and dashed lines are obtained from FT calculations, while the black line is obtained from SC calculations. The bottommost row of figures show how the spin precesses around the axis of rotation as the cone angle α is varied.

First, we checked whether the approximation holds in our case. In order to do this, we have obtained $\delta E_{\rm HE}(\alpha)$ from Eqs. (A1) and (A2) by using the FT for different values of α. We have used 5041 $\mathbf{k}_\parallel$-points in the irreducible Brillouin zone of $MnAu_2$/Ru(0001), while for the freestanding monolayer of $MnAu_2$, 2304 $\mathbf{k}_\parallel$-points are used. The results thus obtained are shown in Fig. 11, where we have plotted $\delta E_{\rm HE}(\alpha)$ as a function of α for both $MnAu_2$/Ru(0001) and a freestanding $MnAu_2$ monolayer. The values obtained from Eqs. (A1) and (A2) are shown by dots and dashed lines, respectively. For both the systems, we see that the values obtained from Eq. (A1) deviate slightly from sinusoidal behavior, but agree qualitatively with the values obtained from Eq. (A2).

Having shown that values of $\delta E_{\rm HE}$ can be calculated approximately by the FT method from Eq. (A2), we proceed to calculate the values self-consistently (SC) using only Eq. (A2). The number of k-points used for these calculations is 800 and 400 for $MnAu_2$/Ru(0001) and freestanding $MnAu_2$, respectively. By comparing the energies obtained for $MnAu_2$/Ru(0001) from SC (black solid line in Fig. 11) and FT (dots and dashed line) methods, we see that the values of $\delta E_{\rm HE}(\alpha)$ do not agree with each other, in fact, they even have opposite sign. On the other hand, for the freestanding monolayer of $MnAu_2$, the values match quite well. This suggests that the FT is applicable for the calculation of $\delta E_{\rm HE}$ between two spin spirals (both conical and planar) of the freestanding $MnAu_2$ monolayer, at least when the difference in wavevectors is small. However, the FT breaks down for $MnAu_2$/Ru(0001) even when α is very small. We conclude that the applicability of the force theorem has to be tested for all cases individually, since the breakdown of the FT for $MnAu_2$/Ru(0001) could not have been anticipated, either from the comparison to the freestanding layers, or to the $FeAu_2$/Ru(0001) case.

ACKNOWLEDGEMENT

Useful discussions with S. Rousset, B. Zimmermann, M. Marathe, B. Schweflinghaus and Ph. Mavropoulos are gratefully acknowledged. S. Biswas acknowledges CSIR, India for a research fellowship and Jülich Supercomputing Centre (JSC) for computation time.

[1] I. E. Dzialoshinskii, Sov. Phys. JETP **5**, 1259 (1957).
[2] T. Moriya, Phys. Rev. **120**, 91 (1960).
[3] S. I. Kiselev, J. C. Sankey, I. N. Krivorotov, N. C. Emley, R. J. Schoelkopf, R. A. Buhrman and D. C. Ralph, Nature (London) **425**, 380 (2003).
[4] I. N. Krivorotov, N. C. Emley, J. C. Sankey, S. I. Kiselev, D. C. Ralph, R. A. Buhrman, Science **307**, 228 (2005).
[5] J. H. Van Vleck, Phys. Rev. **52**, 1178, (1937).
[6] M. Bode, M. Heide, K. von Bergmann, P. Ferriani, S. Heinze, G. Bihlmayer, A. Kubetzka, O. Pietzsch, S. Blügel, and R. Wiesendanger, Nature (London) **447**, 190 (2007).
[7] Y. Yoshida, S. Schröder, P. Ferriani, D. Serrate, A. Kubetzka, K. von Bergmann, S. Heinze, and R. Wiesendanger, Phys. Rev. Lett. **108**, 087205 (2012).
[8] P. Ferriani, K. von Bergmann, E. Y. Vedmedenko, S. Heinze, M. Bode, M. Heide, G. Bihlmayer, S. Blügel, and R. Wiesendanger, Phys. Rev. Lett. **101**, 027201 (2008).
[9] S. Meckler, N. Mikuszeit, A. Preßler, E. Y. Vedmedenko, O. Pietzsch, and R. Wiesendanger, Phys. Rev. Lett. **103**, 157201 (2009).
[10] N. Romming, C. Hanneken, M. Menzel, J. E. Bickel, B. Wolter, K. von Bergmann, A. Kubetzka, and R. Wiesen-

danger, Science **341**, 636 (2013).
[11] L. Pleth Nielsen, F. Besenbacher, I. Stensgaard, E. Lægsgaard, C. Engdahl, P. Stoltze, K. W. Jacobsen, and J. K. Nørskov, Phys. Rev. Lett. **71**, 754 (1993).
[12] M. Marathe, M. Imam, and S. Narasimhan, Phys. Rev. B **79**, 085413 (2009).
[13] J. Tersoff, Phys. Rev. Lett. **74**, 434, (1995).
[14] S. Blügel, Appl. Phys. A **63**, 595 (1996).
[15] S. Mehendale, Y. Girard, V. Repain, C. Chacon, J. Lagoute, S. Rousset, M. Marathe, and S. Narasimhan, Phys. Rev. Lett. **105**, 056101, (2010).
[16] T. Yamada, N. Kunitomi, and Y. Nakai, J. Phys. Soc. Jpn. **28**, 615, (1970).
[17] P. A. Herpin and P. Meriel, J. Phys. Radium, **22**, 337 (1961).
[18] L. Udvardi, S. Khmelevskyi, L. Szunyogh, P. Mohn, and P. Weinberger, Phys. Rev. B **73**, 104446 (2006).
[19] B. Hardrat, A. Al-Zubi, P. Ferriani, S. Blügel, G. Bihlmayer, and S. Heinze, Phys. Rev. B **79**, 094411 (2009).
[20] V. Dupuis, M. Maurer, M. Piecuch, M. F. Ravet, J. Dekoster, S. Andrieu, J. F. Bobo, F. Baudelet, P. Bauer, and A. Fontaine, Phys. Rev. B **48**, 5585 (1993).
[21] S. Biswas and S. Narasimhan, unpublished.
[22] A. Crépieux and C. Lacroix, J. Magn. Magn. Mater. **182**, 341 (1998).
[23] Y. A. Izyumov, Soviet Phys. Uspekhi **27**, 845 (1984).
[24] L. M. Sandratskii, Phys. Status Solidi B **135**, 167 (1986).
[25] A. R. Mackintosh and O. K. Andersen, *Electrons at the Fermi Surface* edited by M. Springford (Cambridge University Press, Cambridge, 1980).
[26] M. Heide, G. Bihlmayer, and S. Blügel, Physica B **404**, 2678, (2009).
[27] For more information see http://www.flapw.de.
[28] J. P. Perdew, K. Burke, and M. Ernzerhof, Phys. Rev. Lett. **77**, 3865 (1996).
[29] A. Al-Zubi, G. Bihlmayer, and S. Blügel, Phys. Status Solidi B **248**, 2242 (2011).
[30] M. Marathe, A. Díaz-Ortiz, and S. Narasimhan, Phys. Rev. B **88**, 245442 (2013).
[31] A. Fert and P. M. Levy, Phys. Rev. Lett. **44**, 1538 (1980).
[32] P. Bruno, Phys. Rev. B **39**, 865 (1989).
[33] M. Ležaić, Ph. Mavropoulos, G. Bihlmayer, and S. Blügel, Phys. Rev. B **88**, 134403 (2013).